Spin Dimer Analysis of the Anisotropic Spin Exchange Interactions in the Distorted Wolframite-Type Oxides $CuWO_4$, $CuMoO_4$-III, and $Cu(Mo_{0.25}W_{0.75})O_4$

Hyun-Joo Koo and Myung-Hwan Whangbo*

Department of Chemistry, North Carolina State University, Raleigh, North Carolina 27695-8204

Received December 27, 2000

The distorted wolframite-type oxides $CuWO_4$ and $CuMoO_4$-III have a structure in which CuO_4 zigzag chains, made up of cis-edge-sharing CuO_6 octahedra, run along the *c*-direction and hence exhibit low-dimensional magnetic properties. We examined the magnetic structures of these compounds and their isostructural analogue $Cu(Mo_{0.25}W_{0.75})O_4$ on the basis of the spin−orbital interaction energies calculated for their spin dimers. Our study shows that these compounds consist of two-dimensional (2D) magnetic sheets defined by one superexchange (intrachain Cu−O−Cu) and three super-superexchange (interchain Cu−O···O−Cu) paths, the strongly interacting spin units of these 2D magnetic sheets are the two-leg antiferromagnetic (AFM) ladder chains running along the $(a + c)$-direction, and the spin arrangement between adjacent AFM ladder chains leads to spin frustration. The similarities and differences in the magnetic structures of $CuWO_4$, $CuMoO_4$-III, and $Cu(Mo_{0.25}W_{0.75})O_4$ were discussed by examining how adjacent AFM ladder chains are coupled via the superexchange paths in the 2D magnetic sheets and how adjacent 2D magnetic sheets are coupled via another superexchange paths along the *c*-direction. Our study reproduces the experimental finding that the magnetic unit cell is doubled along the *a*-axis in $CuWO_4$ and along the *c*-axis in $CuMoO_4$-III and predicts that the magnetic unit cell should be doubled along the *a*- and *b*-axes in $Cu(Mo_{0.25}W_{0.75})O_4$. In the understanding of the strength of a super-superexchange interaction, the importance of the geometrical factors controlling the overlap between the tails of magnetic orbitals was pointed out.

Introduction

Copper tungstate $CuWO_4$ has a distorted wolframite-type structure in which the CuO_4 zigzag chains made up of cis-edge-sharing CuO_6 octahedra are fused by corner-sharing with the WO_4 zigzag chains made up of cis-edge-sharing WO_6 octahedra (Figure 1).[1] All these chains run along the *c*-direction, and the CuO_4 chains possess magnetic ions (i.e., Cu^{2+} ions) while the WO_4 chains do not. Consequently, $CuWO_4$ exhibits low-dimensional magnetic properties. Three decades ago the powder neutron diffraction study of Weitzel[2] showed that $CuWO_4$ undergoes a three-dimensional (3D) antiferromagnetic (AFM) ordering at low temperatures, and its magnetic unit cell is doubled along the *a*-axis. The 3D AFM ordering temperature (i.e., T_N) of $CuWO_4$ was found to be 24(1) K in the EPR study of Anders et al.[3] from the disappearance of the EPR line and 23.0(2) K in the single-crystal neutron diffraction study of Forsyth et al.[4] from the temperature dependence of the magnetic (1/2 0 0) reflection. Doumerc et al.[5] observed that the magnetic susceptibility of $CuWO_4$ exhibits a broad maximum at temperatures far above the 3D ordering temperature (i.e., $T_{max} \approx 90$ K). The latter signals the occurrence of short-range magnetic order well above its long-range ordering temperature, as expected for a low-dimensional magnetic system.

The analysis of the spin exchange interactions of $CuWO_4$ began with the work of Doumerc et al.,[5] who described the temperature-dependence of the magnetic susceptibility in terms of a spin-1/2 one-dimensional (1D) AFM alternating Heisenberg chain. Forsyth et al.[4] suggested that the AFM alternating chains are the CuO_4 zigzag chains running along the *c*-direction and are weakly coupled in the *b*-direction. However, Lake et al.[6] examined the magnetic excitation energies of $CuWO_4$ by inelastic neutron scattering to establish that the AFM alternating chains are not the CuO_4 zigzag chains but run along the [2 −1 0] direction. The superexchange interactions (i.e., interactions via the intrachain Cu−O−Cu bridges) in $CuWO_4$ occur only within each CuO_4 zigzag chain, and there are two different superexchange interactions (i.e., designated as J_1(A) and J_1(B) by Ehrenberg et al.[7]) in the CuO_4 zigzag chain due to the distortion (Figures 1 and 2a). Thus consideration of the super-superexchange interactions (i.e., interactions via the interchain Cu−O···O−Cu linkages) is necessary to explain the occurrence of the AFM alternating chains parallel to [2 −1 0].[7]

The low-lying excited states of an AFM solid are described by a spin Hamiltonian $\hat{H}$ written as a sum of pairwise spin exchange interactions between adjacent spin sites, $-J_{ij}\hat{S}_i \cdot \hat{S}_j$ (here $\hat{S}_i$ and $\hat{S}_j$ are the spin operators at the spin sites *i* and *j*, respectively, and J_{ij} is the spin exchange parameter). The energy spectrum associated with such a phenomenological Hamiltonian is expressed as a function of the parameters J_{ij} and can be used to describe the angle-resolved magnetic excitation energies of an AFM solid obtained from inelastic neutron scattering experiments. From the viewpoint of analyzing results of such experiments, the J_{ij} values are merely numerical fitting param-

(1) Khilborg, L.; Gebert, E. *Acta Crystallogr. B* **1970**, *26*, 1020.
(2) Weitzel, H. *Solid State Commun.* **1970**, *8*, 2071.
(3) Anders, A. G.; Zvyagin, A. I.; Kobets, M. I.; Pelikh, L. N.; Khats'ko, E. N.; Yurko, V. G. *Sov. Phys. JETP* **1972**, *35*, 934.
(4) Forsyth, J. B.; Wilkinson, C.; Zvyagin, A. I. *J. Phys.*: *Condens. Matter* **1991**, *3*, 8433.
(5) Doumerc, J. P.; Dance, J. M.; Chaminade, J. P.; Pouchard, M.; Hagenmuller, P.; Krussanova, M. *Mater. Res. Bull.* **1981**, *16*, 985.
(6) Lake, B.; Tennant, D. A.; Cowley, R. A.; Axe, J. D.; Chen, C. K. *J. Phys.*: *Condens. Matter* **1996**, *8*, 8613.
(7) Ehrenberg, H.; Wiesmann, M.; Garcia-Jaca, J.; Weitzel, H.; Fuess, H. *J. Magn. Magn. Mater*. **1998**, *182*, 152.

10.1021/ic001445r CCC: $20.00 © 2001 American Chemical Society
Published on Web 03/24/2001

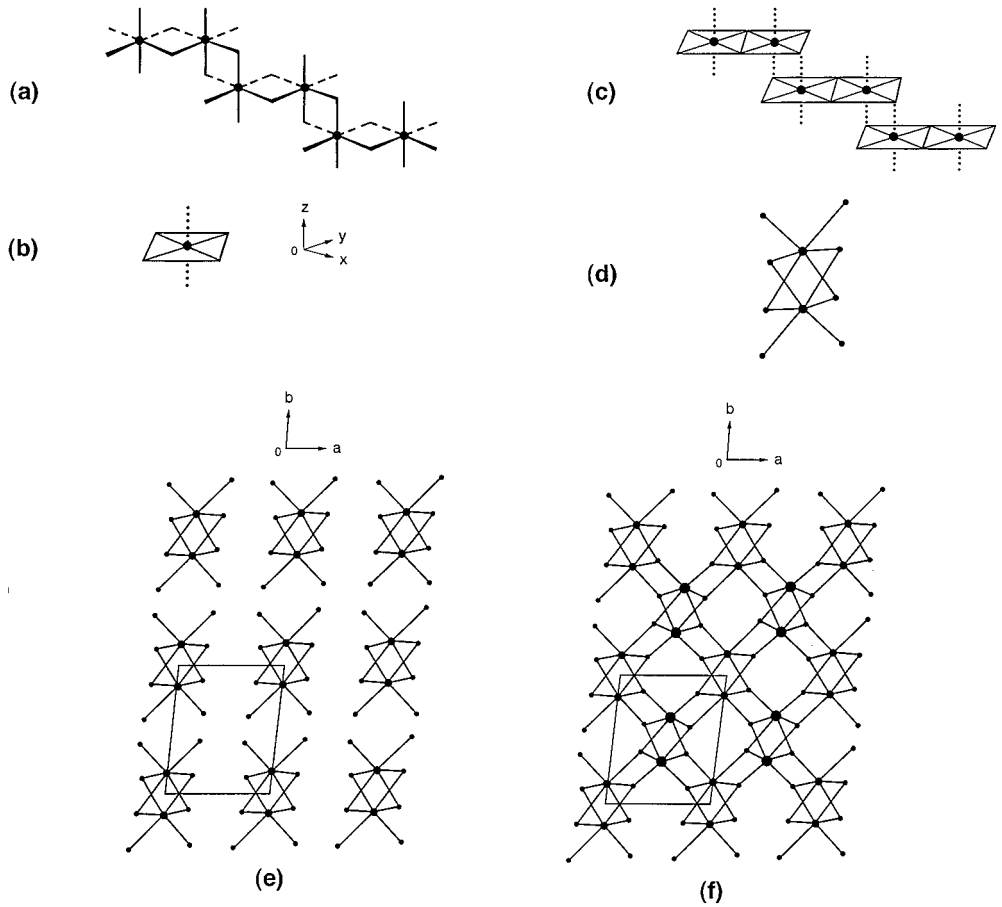

Figure 1. (a) Perspective view of a cis-edge-sharing CuO_4 zigzag chain of $CuWO_4$. (b) Schematic view of the distorted CuO_6 octahedra in $CuWO_4$, where the two long "axial" Cu−O bonds are represented by dotted lines and the four short "equatorial" Cu−O bonds by solid lines. (c) Perspective view of a cis-edge-sharing CuO_4 zigzag chain of $CuWO_4$ showing the distortions of the CuO_6 octahedra explicitly. (d) Schematic projection view of a cis-edge-sharing CuO_4 zigzag chain of $CuWO_4$ along the *c*-direction, where the larger and smaller circles represent Cu and O atoms, respectively. (e) Schematic projection view of the CuO_4 zigzag chains in $CuWO_4$ along the *c*-direction. (f) Schematic projection view of the CuO_4 and WO_4 zigzag chains in $CuWO_4$ along the *c*-direction, where large, medium, and small circles represent W, Cu, and O atoms, respectively.

eters so that in principle experimental results can be reproduced by more than one set of spin exchange parameters. Indeed, Lake et al.[6] reported that the magnetic excitation energies of $CuWO_4$ are simulated equally well by two different sets of spin exchange parameters (*model 1* and *model 2*).

The question of which model of spin exchange parameters is appropriate for $CuWO_4$ was examined in the neutron powder diffraction study of Ehrenberg et al.,[7] who compared the magnetic structures of $CuWO_4$ and its molybdenum analogue, $CuMoO_4$-III, from the viewpoints of their super-superexchange paths. (There are five different forms of $CuMoO_4$ reported in the literature,[7−12] and $CuMoO_4$-III is isostructural with $CuWO_4$.) They showed that $CuMoO_4$-III undergoes a 3D AFM ordering as does $CuWO_4$, but its magnetic unit cell is doubled along the *c*-axis unlike the case of $CuWO_4$. Since the strength of a spin exchange interaction is expected to depend continuously on geometrical details of the exchange path, Ehrenberg et al. reasoned that the dominant spin exchange interactions of $CuWO_4$ and $CuMoO_4$-III must be similar and result in AFM alternating chains parallel to [2 −1 0]. By considering only the super-superexchange paths with Cu−O distances smaller than 2.3 Å and ∠Cu−O···O angles larger than 110°, they identified three dominant spin exchange paths (designated as J_6(B), J_8, and J_9(A)) (Figure 3a) that are common to both compounds and lead to AFM arrangements in both compounds. Ehrenberg et al. noted that these spin exchange paths are consistent with model 1 of Blake et al. but not with their model 2. Concerning the difference between $CuWO_4$ and $CuMoO_4$-III, they suggested that the AFM alternating chains along [2 −1 0] formed by J_6(B) and J_9(A) are coupled via J_8 to form two-dimensional (2D) magnetic sheets (Figure 3a) in both compounds and these sheets are coupled via the superexchange paths J_1(B) ferromagnetically in $CuWO_4$ but antiferromagnetically in $CuMoO_4$-III (Figure 2b,c).

Thus, Ehrenberg et al.[7] provided strong evidence that the spin exchange interactions of model 1 are appropriate for both $CuWO_4$ and $CuMoO_4$-III, although their reasoning is based on geometrical considerations and the comparison of the magnetic structures of the two compounds. To confirm their conclusion unambiguously, it is necessary to examine the spin exchange interactions of the two compounds on the basis of energy considerations. Furthermore, we note that the superexchange paths J_1(A) present in the CuO_4 zigzag chains make triangular arrangements with the super-superexchange paths J_6(B) and J_8 in each 2D magnetic sheet (Figure 3a). The ∠Cu−O−Cu angle

(8) Wiesmann, M.; Ehrenberg, H.; Miehe, G.; Peun, T.; Weitzel, H.; Fuess, H. *J. Solid State Chem.* **1997**, *132*, 88 and references therein.
(9) Abrahams, S. C.; Bernstein, J. L.; Jamieson, P. B. *J. Chem. Phys.* **1968**, *48*, 2619.
(10) Weber, T.; Harz, M.; Wehner, B.; Zahn, G.; Paufler, P. *Z. Kristallogr.* **1998**, *213*, 210.
(11) Ehrenberg, H.; Weitzel, H.; Paulus, H.; Wiesmann, M.; Wltschek, G.; Gesselle, M.; Fuess, H. *J. Phys. Chem. Solids* **1997**, *58*, 153.
(12) Tali, R.; Tabachenko, V. V.; Kovba, L. M.; Dem'yanets, L. N. *Russ. J. Inorg. Chem.* **1991**, *36*, 927.

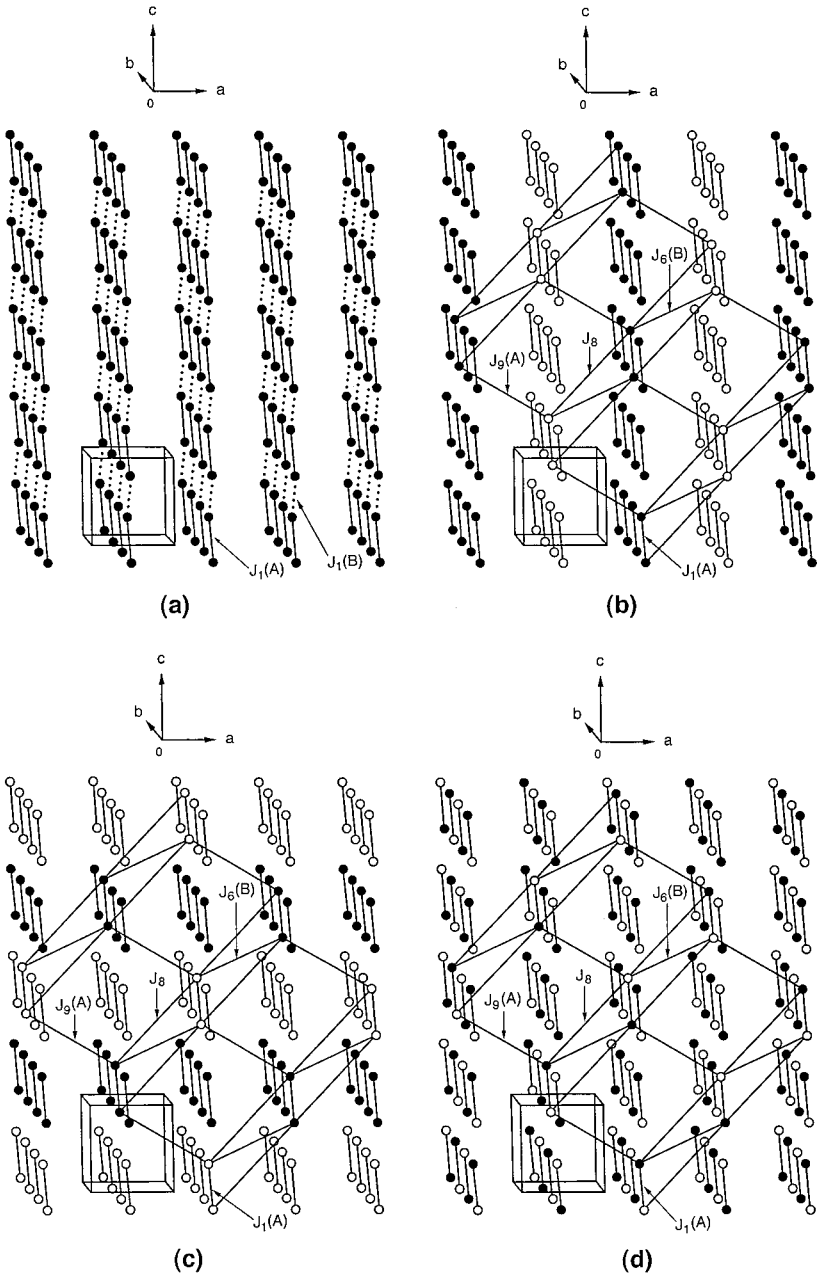

Figure 2. (a) Perspective view of the Cu^{2+} ion arrangement in $CuWO_4$, where the CuO_4 zigzag chains appear as zigzag chains of Cu^{2+} ions with alternating superexchange paths J_1(A) and J_1(B) (represented by the solid and dotted lines, respectively). (b) Perspective view of the Cu^{2+} ion arrangement in $CuWO_4$, where a single 2D magnetic sheet defined by the exchange paths J_1(A), J_6(B), J_8, and J_9(A) are indicated by solid lines. (c) Perspective view of the Cu^{2+} ion arrangement in $CuMoO_4$-III, where a single 2D magnetic sheet defined by the exchange paths J_1(A), J_6(B), J_8, and J_9(A) are indicated by solid lines. (d) Perspective view of the Cu^{2+} ion arrangement expected for $Cu(Mo_{0.25}W_{0.75})O_4$, where a single 2D magnetic sheet defined by the exchange paths J_1(A), J_6(B), J_8, and J_9(A) are indicated by solid lines. In (b)−(d), the exchange paths J_1(B) are not shown for simplicity, and the filled and empty circles are used to represent the Cu^{2+} ion sites with up- and down-spins, respectively.

of the superexchange path J_1(A) is considerably larger than 90° (Tables 2−4) so that the superexchange path J_1(A) should prefer an AFM arrangement.[13] Therefore it is crucial to consider magnetic frustrations resulting from the triangular arrangements of J_1(A), J_6(B), and J_8 and hence their effect on the magnetic ordering in each 2D magnetic sheet. Finally, the single-crystal X-ray diffraction study of Wiesmann et al.[8] showed that the "mixed" crystal $Cu(Mo_{0.25}W_{0.75})O_4$ is isostructural with $CuWO_4$ and $CuMoO_4$-III. So far the magnetic structures of $Cu(Mo_{0.25}W_{0.75})O_4$ have not been determined. Thus it would be important to predict them. In the present work we probe these questions on the basis of spin dimer analysis, which has been found to be quite successful in explaining the qualitative trends in the spin exchange interactions of various extended AFM solids.[14−19] In the following, we analyze the reported crystal structures of $CuWO_4$, $CuMoO_4$-III, and $Cu(Mo_{0.25}W_{0.75})O_4$, identify their spin dimers (i.e., structural units containing two adjacent spin sites), calculate their spin−orbital interaction

(13) Goodenough, G. *Magnetism and the Chemical Bond*; Interscience: New York, 1963.

(14) Lee, K. S.; Koo, H.-J.; Whangbo, M.-H. *Inorg. Chem.* **1999**, *38*, 2199.
(15) Koo, H.-J.; Whangbo, M.-H. *Solid State Commun.* **1999**, *111*, 353.
(16) Whangbo, M.-H.; Koo, H.-J.; Lee, K. S. *Solid State Commun.* **2000**, *114*, 27.
(17) Koo, H.-J.; Whangbo, M.-H. *J. Solid State Chem.* **2000**, *151*, 96.
(18) Koo, H.-J.; Whangbo, M.-H. *J. Solid State Chem.* **2000**, *153*, 263.
(19) Koo, H.-J.; Whangbo, M.-H. *Inorg. Chem.* **2000**, *39*, 3599.

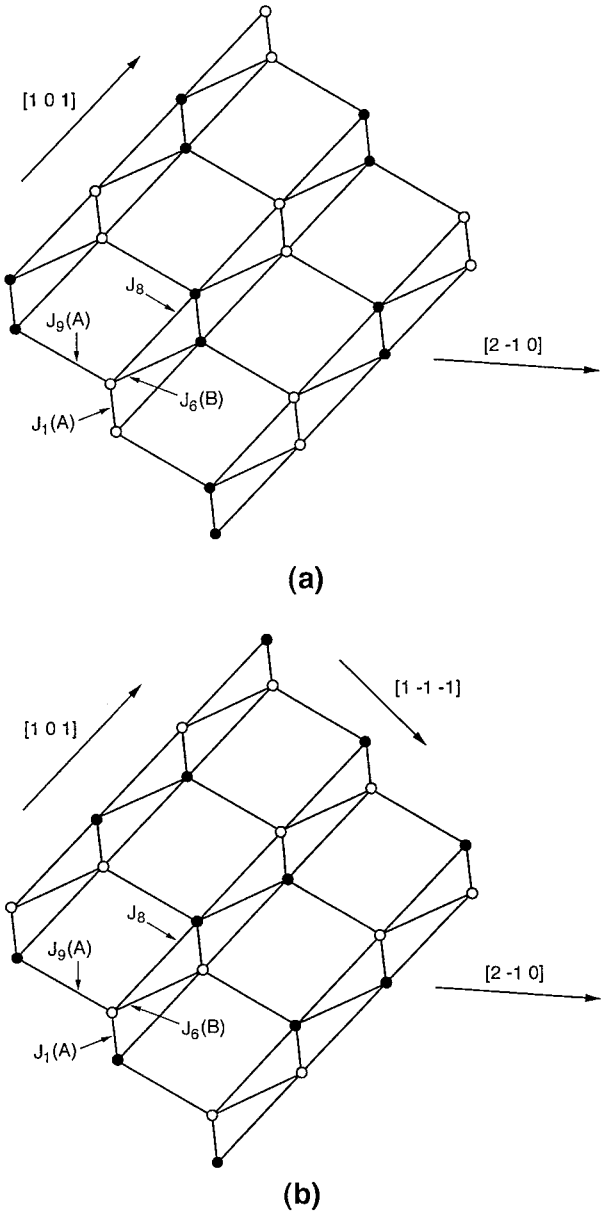

Figure 3. (a) Perspective view of the 2D magnetic sheet present in $CuWO_4$ and $CuMoO_4$-III, which is defined by the exchange paths J_1-(A), J_6(B), J_8, and J_9(A). (b) Perspective view of the 2D magnetic sheet predicted to be present in $Cu(Mo_{0.25}W_{0.75})O_4$, which is defined by the exchange paths J_1(A), J_6(B), J_8, and J_9(A). In (a) and (b) the filled and empty circles are used to represent the Cu^{2+} ion sites with up- and down-spins, respectively.

energies (see below), and discuss the magnetic structures of these compounds.

Arrangements of the Superexchange and Super-Superexchange Paths

Single-crystal X-ray structures are known for $CuWO_4$,[1] $CuMoO_4$-III,[12] and $Cu(Mo_{0.25}W_{0.75})O_4$.[8] The structure of $CuWO_4$ was also determined by single-crystal neutron diffraction measurements,[4] and that of $CuMoO_4$-III by neutron powder diffraction measurements.[7] In the three compounds $CuWO_4$, $CuMoO_4$-III, and $Cu(Mo_{0.25}W_{0.75})O_4$, the structures of the CuO_4 zigzag chains are similar, and so are their 3D arrangements. Thus in the following description of the CuO_4 zigzag chains and their 3D arrangement, we will refer only to the crystal structure of $CuWO_4$.

Table 1. Exponents ζ_i and Valence Shell Ionization Potentials H_{ii} of Slater-Type Orbitals χ_i Used for Extended Hückel Tight-Binding Calculation[a]

atom	χ_i	H_{ii} (eV)	ζ_i	c_1[b]	ζ_i'	c_2[b]
Cu	4s	−11.4	2.151	1.0		
Cu	4p	−6.06	1.370	1.0		
Cu	3d	−14.0	7.025	0.4473	3.004	0.6978
O	2s	−32.3	2.688	0.7076	1.675	0.3745
O	2p	−14.8	3.694	0.3322	1.659	0.7448

[a] H_{ii}'s are the diagonal matrix elements $\langle\chi_i|H^{eff}|\chi_i\rangle$, where H^{eff} is the effective Hamiltonian. In our calculations of the off-diagonal matrix elements $H^{eff} = \langle\chi_i|H^{eff}|\chi_j\rangle$, the weighted formula was used. See: Ammeter, J.; Bürgi, H.-B.; Thibeault, J.; Hoffmann, R. *J. Am. Chem. Soc*. **1978**, *100*, 3686. [b] Coefficients used in the double-ζ Slater-type orbital expansion.

Figure 1a shows a perspective view of a cis-edge-sharing CuO_4 zigzag chain made up of distorted CuO_6 octahedra. Each CuO_6 octahedron shows an "axial" elongation of two *trans*-Cu−O bonds due to a Jahn−Teller distortion. The oxygen atoms of the two long "axial" Cu−O bonds may be represented by dotted lines (i.e., Cu···O), and those of the four short "equatorial" Cu−O bonds by solid lines (i.e., Cu−O) as depicted in Figure 1b. (The plane of the four "equatorial" Cu−O bonds will be referred to as the "equatorial" plane.) Then, the CuO_4 zigzag chains of $CuWO_4$ have the distortion pattern shown in Figure 1c, which reveals two different spin exchange interactions that occur via the superexchange paths: one with two Cu−O−Cu bridges (i.e., J_1(A)) and the other with two Cu−O···Cu bridges (i.e., J_1(B)). To facilitate the description of the 3D crystal structure of $CuWO_4$, we present the CuO_4 zigzag chain of Figure 1a as the projection view along the chain direction (i.e., the *c*-direction), as depicted in Figure 1d, where all the Cu atoms of the zigzag chain are projected onto two separate positions. Then a projection view of the CuO_4 zigzag chains of $CuWO_4$ along the *c*-direction can be represented as in Figure 1e. In Figure 1e there exists a zigzag chain of empty octahedral sites at the center of every four adjacent CuO_4 zigzag chains in parallogram arrangement. When W atoms occupy such empty sites, a WO_4 zigzag chain results from each chain of octahedral sites. A projection view of the CuO_4 and WO_4 zigzag chains of $CuWO_4$ along the *c*-direction can be represented as in Figure 1f. Thus one WO_4 zigzag chain shares its oxygen atoms with four different CuO_4 zigzag chains. Likewise, one CuO_4 zigzag chain shares its oxygen atoms with four different WO_4 zigzag chains.

A perspective view of the Cu^{2+} cation arrangement in $CuWO_4$ is shown in Figure 2a, where the superexchange paths J_1(A) and J_1(B) are indicated by solid and dotted lines, respectively. The same view is presented in Figure 2b, where a single 2D magnetic sheet defined by the exchange paths J_1(A), J_6(B), J_8, and J_9(A) is drawn in by solid lines and the Cu^{2+} cation sites with up- and down-spins are depicted by filled and empty circles, respectively. Figure 3a shows a perspective view of the 2D magnetic sheet, where the AFM alternating chains made up of J_9(A) and J_6(B) run along [2 −1 0] and are coupled by the exchange paths J_8. In $CuWO_4$ such 2D magnetic sheets stack along the *c*-direction such that adjacent 2D magnetic sheets interact via the superexchange paths J_1(B), as shown in Figure 2b.

Spin Dimers and Spin−Orbital Interaction Energies

The spin monomers of $CuWO_4$ (i.e., the structural units containing single spin sites) are the octahedral clusters $(CuO_6)^{10-}$

Table 2. Δe Values (in meV), Cu···Cu, Cu—O, and O···O Distances (in Å), and ∠Cu−O−Cu and ∠Cu-O···O Angles (deg) Associated with Spin Dimers in $CuWO_4$

exchange path	Δe	Cu···Cu	bridge	
(a) Crystal Structure of Khilborg and Gebert[1]				
superexchange (intrachain)			Cu—O—Cu	(∠Cu−O−Cu)
J_1(A)	48	2.986	1.978, 1.997	(97.37)
J_1(B)	13	3.150	1.967, 2.451	(90.29)
super-superexchange (interchain)			Cu—O···O—Cu	(∠Cu−O···O)
J_6(B)	49	5.408	1.967, 2.834, 1.967	(104.91, 104.91)
			1.967, 2.826, 1.997	(159.24, 104.32)
J_8	77	6.629	1.967, 2.826, 1.978	(159.24, 154.48)
J_9(A)	204	6.283	1.961, 2.411, 1.961	(165.10, 165.10)
(b) Crystal structure Structure of Forsyth et al.[4]				
superexchange (intrachain)			Cu—O—Cu	(∠Cu−O−Cu)
J_1(A)	52	2.986	1.980, 1.992	(97.47)
J_1(B)	14	3.141	1.959, 2.434	(90.64)
super-superexchange (interchain)			Cu—O···O—Cu	(∠Cu−O···O)
J_6(B)	47	5.401	1.959, 2.832, 1.959	(105.19, 105.19)
			1.959, 2.831, 1.992	(159.16, 104.24)
J_8	76	6.625	1.959, 2.831, 1.980	(159.16, 154.43)
J_9(A)	198	6.279	1.952, 2.424, 1.952	(165.44, 165.44)

Table 3. Δe Values (in meV), Cu···Cu, Cu—O, and O···O Distances (in Å), and ∠Cu−O−Cu and ∠Cu-O···O Angles (deg) Associated with Spin Dimers in $CuMoO_4$-III

exchange path	Δe	Cu···Cu	bridge	
(a) Crystal Structure of Tali et al.[12]				
superexchange (intrachain)			Cu—O—Cu	(∠Cu−O−Cu)
J_1(A)	40	2.967	1.973, 1.977	(97.38)
J_1(B)	20	3.106	1.971, 2.453	(88.49)
super-superexchange (interchain)			Cu—O···O—Cu	(∠Cu−O···O)
J_6(B)	48	5.409	1.971, 2.804, 1.971	(105.34, 105.34)
			1.971, 2.839, 1.977	(160.10, 103.93)
J_8	75	6.642	1.971, 2.839, 1.973	(160.10. 154.05)
J_9(A)	205	6.232	1.933, 2.410, 1.933	(166.03, 166.03)
(b) Crystal Structure of Ehrenberg et al.[7]				
superexchange (intrachain)			Cu—O—Cu	(∠Cu−O−Cu)
J_1(A)	47	2.977	1.968, 1.973	(98.12)
J_1(B)	22	3.098	1.955, 2.428	(89.32)
super-superexchange (interchain)			Cu—O···O—Cu	(∠Cu−O···O)
J_6(B)	47	5.373	1.955, 2.822, 1.955	(104.76, 104.76)
			1.955, 2.848, 1.968	(158.76, 103.48)
J_8	73	6.625	1.955, 2.848, 1.973	(158.76, 153.70)
J_9(A)	214	6.225	1.933, 2.394, 1.933	(167.61, 167.61)

Table 4. Δe Values (in meV), Cu···Cu, Cu—O, and O···O Distances (in Å), and ∠Cu−O−Cu and ∠Cu-O···O Angles (deg) Associated with Spin Dimers in $Cu(Mo_{0.25}W_{0.75})O_4$

exchange path	Δe	Cu···Cu	bridge	
superexchange (intrachain)			Cu—O—Cu	(∠Cu−O−Cu)
J_1(A)	82	3.067	2.009, 2.019	(99.16)
J_1(B)	22	3.057	1.921, 2.432	(88.39)
super-superexchange (interchain)			Cu—O···O—Cu	(∠Cu−O···O)
J_6(B)	40	5.366	1.921, 2.833, 1.921	(106.00, 106.00)
			1.921, 2.841, 2.009	(160.39, 103.22)
J_8	74	6.636	1.921, 2.841, 2.019	(160.39, 153.57)
J_9(A)	214	6.214	1.922, 2.427, 1.922	(166.80, 166.80)

containing Cu^{2+} (d^9) cations. If we choose the "idealized" local coordinate system for a distorted CuO_6 octahedron such that the equatorial Cu—O bonds are pointed along the *x*- and *y*-axes (Figure 1b), then the unpaired spin of each monomer resides in the magnetic orbital in which the x^2-y^2 orbital of Cu is combined out-of-phase with the oxygen 2p orbitals in the "equatorial" plane as depicted in Figure 4a. In other words, the magnetic orbital is extended from the Cu to the equatorial oxygen ligands, so that the small p-orbitals on the equatorial oxygen atoms are the "tails" of the magnetic orbital. The spin dimers with superexchange paths occur within each CuO_4 zigzag chain and are given by $(Cu_2O_{10})^{16-}$ cluster ions composed of two edge-sharing CuO_6 octahedra. In these "intrachain" spin dimers the Cu atoms interact via the Cu−O−Cu superexchange paths. The spin dimers with super-superexchange paths occur between adjacent CuO_4 zigzag chains and are given by $(Cu_2O_{12})^{20-}$ cluster ions made up of two isolated $(CuO_6)^{10-}$ ions. In these "interchain" spin dimers the Cu atoms interact via the Cu—O···O—Cu super-superexchange paths. To see if the interaction between the spin monomers of an interchain spin dimer is affected by the MO_6 (M = Mo, W) octahedra bridging the two spin monomers, one may also define an interchain spin dimer as the $(Cu_2O_{12})^{20-}$ ion plus all the MO_6 octahedra that link the two Cu^{2+} ions via Cu−O−M−O−Cu bridges.

For a spin dimer consisting of a single unpaired electron/spin site, the spin exchange parameter *J* is equal to the energy difference ΔE between the triplet and singlet states of the spin dimer, i.e., $J = \Delta E = {}^1E - {}^3E$, where ${}^1E$ and ${}^3E$ are the total

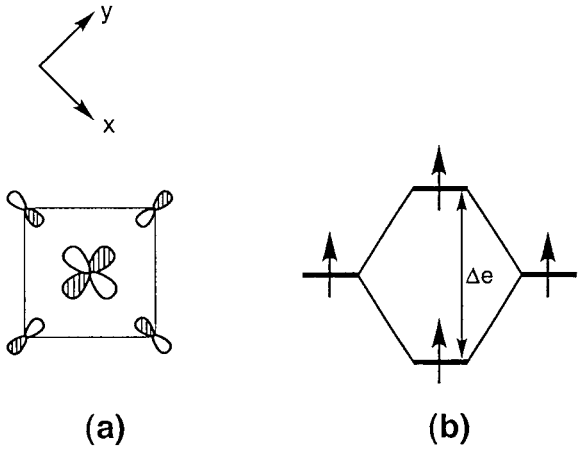

Figure 4. (a) Magnetic orbital of an axially elongated octahedral cluster $(CuO_6)^{10-}$, in which the x^2-y^2 orbital of the Cu atom is combined out-of-phase with the p orbitals of the O atoms in the equatorial plane. (b) Spin−orbital interaction energy of a spin dimer made up of two crystallographically equivalent spin sites.

energies of the singlet and triplet states, respectively. The quantitative evaluation of the total energy difference ΔE on the basis of first-principles electronic structure calculations requires state-of-the-art computational efforts on the basis of either configuration interaction wave functions or density functional theory (DFT).[20,21] Within DFT, the spin exchange parameter of a spin dimer can also be calculated in terms of the orbital energy difference between the up- and down-spin magnetic orbitals calculated for the "transition state" of the spin dimer.[22] A spin dimer of an extended solid is defined as a cluster obtained by breaking the bonds linking the spin dimer to the crystal lattice and then replacing each broken bond with an unshared electron pair belonging to the spin dimer (see above). Thus as an object for electronic structure calculations, a spin dimer becomes a highly charged anion cluster. In first-principles electronic structure calculations, this unphysical situation is corrected by surrounding an isolated spin dimer with a set of point positive charges (at the cation positions of the lattice around the spin dimer) such that the resulting attractive potential removes the unphysical effect of the high negative charge.[23] To deduce spin exchange parameters of an extended magnetic solid without doing calculations for isolated spin dimers, one may carry out electronic band structure calculations based on DFT for various ordered spin arrangements of the magnetic solid. Then spin exchange parameters are deduced by projecting the electronic energy differences between these spin states into the corresponding energy differences associated with a model spin Hamiltonian expressed in terms of the spin exchange parameters to be determined.[24] Regardless of which approach is employed, quantitative calculations of spin exchange parameters using first-principles electronic structure calculations become difficult to apply to extended magnetic solids with large and complex unit cells. To analyze the spin exchange interactions of such systems, it is necessary to rely on a qualitative approach,[25,26] which is discussed below.

The spin exchange parameter of a spin dimer can be expressed as $J = J_F + J_{AF}$, where J_F (>0) and J_{AF} (<0) are the ferromagnetic and antiferromagnetic terms, respectively. When the two spin sites of a spin dimer are represented by nonorthogonal magnetic orbitals ϕ_1 and ϕ_2, the ferromagnetic term is given by $J_F = 2K_{12}$, where K_{12} is the exchange repulsion between the two magnetic orbitals (i.e., the Coulomb repulsion resulting from the overlap electron density distribution $\phi_1\phi_2$).[25] The antiferromagnetic term is expressed as $J_{AF} = -2S\Delta e$, where S is the overlap integral between ϕ_1 and ϕ_2 and Δe is the energy separation between the highest two singly occupied energy levels of a spin dimer (Figure 4b). Due to the relationship $\Delta e \approx S$, the J_{AF} value is proportional to the square of the spin−orbital interaction energy Δe, i.e., $J_{AF} \approx -(\Delta e)^2$.[25,26] As shown recently,[14−19] the qualitative trends in the J parameters of extended AFM solids are explained in terms of the spin−orbital interaction energies calculated for their spin dimers using the extended Hückel method.[27,28] It is noted that the electronic structure of a system obtained by extended Hückel calculations does not depend on the number of electrons the system has. This is a weakness as well as a strength of this method, as reviewed recently.[29] In contrast to the case of first-principles electronic structure calculations, therefore, the high negative charge of a spin dimer has no unphysical effect on extended Hückel electronic structure calculations.

Calculations

Table 1 summarizes the atomic orbital parameters of Cu and O used in our extended Hückel molecular orbital calculations for the Δe values of various spin dimers. The 3d orbitals of Cu and the 2s/2p orbitals of O are represented by double-ζ Slater type orbitals,[30] because such orbitals reproduce well the trends in the anisotropic spin exchange interactions of magnetic transition metal oxides and fluorides.[14−19]

The Δe values calculated for the spin dimers corresponding to the spin-exchange paths J_1(A), J_1(B), J_6(B), J_8, and J_9(A) of $CuWO_4$, $CuMoO_4$-III, and $Cu(Mo_{0.25}W_{0.75})O_4$ are listed in Tables 2−4, respectively. These tables also summarize the Cu···Cu, Cu−O, and O···O distances as well as the ∠Cu−O−Cu and ∠Cu−O···O angles associated with the spin-exchange paths. For the super-superexchange paths, only the Cu−O and O···O distances and the ∠Cu−O···O angles associated with short O···O contacts are listed. For each of $CuWO_4$, $CuMoO_4$-III, and $Cu(Mo_{0.25}W_{0.75})O_4$, the spin dimers for spin-exchange paths different from the five paths J_1(A), J_1(B), J_6(B), J_8, and J_9(A) are all calculated to have Δe values smaller than that calculated for J_1(B), the weakest exchange path among the five. Thus, they are not listed in Tables 2−4.

The Δe values of the interchain spin dimers listed in Tables 2−4 were calculated without the MO_6 octahedra that link the two Cu^{2+} ions via Cu−O-M−O−Cu bridges, because those calculated with bridging MO_6 octahedra give very similar results. Nevertheless, it should be pointed out that calculations for an interchain spin dimer with extra O−M−O bridges can overestimate the Δe values for weak super-superexchange paths and hence lead to unphysical results.[18,31]

The two reported crystal structures of $CuWO_4$ provide essentially the same Δe values for J_1(A), J_1(B), J_6(B), J_8, and J_9(A) (Table 2). The same is found for the two reported structures of $CuMoO_4$-III (Table 3).

(20) For a recent review, see: Illas, F.; Moreira, I. d. P. R.; de Graaf, C.; Barone, V. *Theor. Chem. Acc.* **2000**, *104*, 265.
(21) Noodleman, L. *J. Chem. Phys.* **1981**, *74*, 5737.
(22) Dai, D.; Whangbo, M.-H. *J. Chem. Phys.*, in press.
(23) Derenzo, S. E.; Klitenberg, M. K.; Weber, M. J. *J. Chem. Phys.* **2000**, *112*, 2074 and references therein.
(24) For example, see: Chartier, A.; D'Arco, P.; Dovesi, R.; Saunders: V. R. *Phys. Rev. B* **1999**, *20*, 14042.
(25) Kahn, O. *Molecular Magnetism*; VCH Publishers: Weinheim, Germany, 1993.
(26) Hay, P. J.; Thibeault, J. C.; Hoffmann, R. *J. Am. Chem. Soc.* **1975**, *97*, 4884.
(27) Hoffmann, R. *J. Chem. Phys.* **1963**, *39*, 1397.
(28) Our calculations were carried out by employing the *CAESAR* program package (Ren, J.; Liang, W.; Whangbo, M.-H. *Crystal and Electronic Structure Analysis Using CAESAR*, 1998; http://www.PrimeC.com/).
(29) Whangbo, M.-H. *Theor. Chem. Acc.* **2000**, *103*, 252.
(30) Clementi, E.; Roetti, C. *At. Data Nucl. Data Tables* **1974**, *14*, 177.
(31) Koo, H.-J.; Whangbo, M.-H. *J. Solid State Chem.*, in press.

Magnetic Structures of $CuWO_4$ and $CuMoO_4$-III

Tables 2 and 3 show that J_6(B), J_8, and J_9(A) are the three strongest super-superexchange paths for both $CuWO_4$ and $CuMoO_4$-III, in support of Ehrenberg et al.'s conclusion.[7] Of the five exchange paths J_1(A), J_1(B), J_6(B), J_8,and J_9(A), the smallest Δe value is found for J_1(B). This also supports Ehrenberg et al.'s picture that $CuWO_4$ and $CuMoO_4$-III consist of weakly interacting 2D magnetic sheets made up of J_6(B), J_8, and J_9(A). The fact that the spin exchange interaction is stronger for J_9(A) than for J_6(B) is in agreement with the spin exchange parameters (i.e., -33.26 and -8.34 meV, respectively, using the convention that a negative J means an AFM coupling) estimated by Lake et al.[6]

However, the Δe values of Tables 2 and 3 reveal that the 2D magnetic sheets of $CuWO_4$ and $CuMoO_4$-III have more complex magnetic structures than those envisioned by Ehrenberg et al.[7] and Blake et al.[6,32,33] For each compound, the Δe values decrease in the following order: $J_9(A) \gg J_8 > J_6(B)$, $J_1(A) > J_1(B)$. Since the Δe value for the superexchange path J_1(A) is nearly the same as that for the super-superexchange path J_6(B), it is not justified to neglect the superexchange path J_1(A) in describing the magnetic structures of $CuWO_4$ and $CuMoO_4$-III. Furthermore, the Δe value for the path J_8, which couples the AFM alternating chains defined by J_9(A) and J_6(B), is larger than that for the path J_6(B). Consequently, the strongly interacting spin units (SISU's) of $CuWO_4$ and $CuMoO_4$-III are not the AFM alternating chains parallel to [2 −1 0] but the "two-leg AFM ladder chains" made up of J_9(A) and J_8 running along [1 0 1] (Figure 3a). This means that the broad maximum in the magnetic susceptibility of $CuWO_4$ at $T_{max} \approx 90$ K, which signals fluctuation of magnetic order in 1D chains, is not caused by the AFM alternating chains along [2 −1 0] but by the AFM ladder chains along [1 0 1].

Let us now consider the 2D magnetic sheets of $CuWO_4$ and $CuMoO_4$-III in terms of the AFM ladder chains. In a given 2D magnetic sheet, adjacent AFM ladder chains interact via the superexchange path J_1(A) and the super-superexchange path J_6-(B). These two paths make triangular arrangements with the super-superexchange path J_8, thereby leading to magnetic frustration. In principle, therefore, there are two different ways of arranging the AFM ladder chains to form a 2D magnetic sheet, as depicted in Figure 3a,b. In the 2D magnetic arrangement of Figure 3a (hereafter referred to as 2D−F spin arrangement), the AFM ladder chains are coupled ferromagnetically via the superexchange paths J_1(A) so that the super-superexchange paths J_6(B) have AFM arrangements. In the 2D magnetic arrangement of Figure 3b (hereafter referred to as 2D−A spin arrangement), the AFM ladder chains are coupled antiferromagnetically via the superexchange paths J_1(A) so that the super-superexchange paths J_6(B) have ferromagnetic arrangements. Experimentally, the 2D magnetic sheets of $CuWO_4$ and $CuMoO_4$-III are found to have the 2D−F spin arrangement.

In view of the fact that the paths J_1(A) and J_6(B) have similar Δe values, it is important to consider why the 2D−F spin arrangement is favored over the 2D−A spin arrangement. Because $J_{AF} \approx -(\Delta e)^2$, the two paths should have similar J_{AF} values. The spin exchange parameter J is composed of two opposing terms, i.e., $J = J_F + J_{AF}$, so that the comparison of the relative magnitudes of J values in terms of the J_{AF} terms alone (equivalently, in terms of the Δe values alone) can be misleading unless the J_F terms are either zero or constant. This requirement is not met when exchange paths of different kinds (e.g., the superexchange versus the super-superexchange paths) are compared. The J_F term of a spin dimer is proportional to the Coulomb repulsion associated with the overlap electron density distribution $\phi_1\phi_2$ of its two magnetic orbitals ϕ_1 and ϕ_2. As already mentioned, the magnetic orbital in the equatorial plane (Figure 4a) has p-orbital "tails" on the equatorial oxygen ligands. In a superexchange (Cu−O−Cu) path such as J_1(A) the bridging oxygen atoms provide p-orbital tails to both Cu^{2+} ions so that the overlap electron density distribution $\phi_1\phi_2$ is not negligible around the bridging oxygen atoms, which makes the J_F term nonnegligible. Consequently, for the J_1(A) path, the magnitude of J would be reduced from that of J_{AF} due to the opposing effect of the J_F term. For a super-superexchange path such as J_6(B), however, the overlap density distribution and the associated J_F term should be negligible because no oxygen atom is a common ligand to both Cu^{2+} ions of the interchain spin dimer, so that the J value would be close to J_{AF}. Therefore, given that the paths J_1(A) and J_6(B) have similar Δe values, the super-superexchange path J_6(B) provides a stronger AFM coupling than does the superexchange path J_1(A). This explains why the 2D magnetic sheets of $CuWO_4$ and $CuMoO_4$-III favor the 2D−F spin arrangement over the 2D−A spin arrangement. It is erroneous to infer from the 2D−F spin arrangement that the superexchange path J_1(A) has an inherent tendency to couple spins ferromagnetically. From the consideration of the ∠Cu−O−Cu angle involved (Tables 2 and 3), this exchange path is expected to prefer an AFM coupling. In the 2D−F spin arrangement the J_1(A) paths have ferromagnetic arrangements simply because the path J_1(A) provides the weakest AFM coupling in the triangular arrangement of J_1(A), J_6(B), and J_8.

Let us now consider the difference between $CuWO_4$ and $CuMoO_4$-III in their magnetic structures. Ehrenberg et al.[7] pointed out that the two compounds are the same in the magnetic structure of their individual 2D magnetic sheets but differ in how adjacent 2D magnetic sheets interact via the superexchange paths J_1(B): the J_1(B) coupling between adjacent 2D magnetic sheets is ferromagnetic in $CuWO_4$ (Figure 2b) but antiferromagnetic in $CuMoO_4$-III (Figure 2c). Our calculations are consistent with this conclusion, because the J_1(B) path has a larger Δe value (by a factor of approximately 2) and, hence, provides a stronger tendency for AFM coupling in $CuMoO_4$-III than in $CuWO_4$. From Figure 2b,c, it is clear that the ferromagnetic J_1(B) coupling doubles the magnetic unit cell along the *a*-axis in $CuWO_4$, whereas the antiferromagnetic J_1-(B) coupling doubles the magnetic unit cell along the *c*-axis in $CuMoO_4$-III.

Probable Magnetic Structure of $Cu(Mo_{0.25}W_{0.75})O_4$

Table 4 shows that the Δe values of the five exchange paths decrease in the following order: $J_9(A) \gg J_1(A)$, $J_8 > J_6(B) > J_1(B)$. According to our discussion presented in the previous section, the superexchange path J_1(A) has a nonnegligible J_F term but the super-superexchange path J_8 does not. Since the Δe value of J_1(A) is only slightly larger than that of J_8, it is probable that the J_8 path provides a slightly stronger AFM coupling than does the J_1(A) path. However, the J_1(A) path should provide a much stronger AFM coupling than does the J_6(B) path, because the Δe value of J_1(A) is much larger than that of J_6(B) (by a factor of 2). Consequently, the SISU's of $Cu(Mo_{0.25}W_{0.75})O_4$ should also be given by the two-leg AFM ladder chains, but these ladder chains would have the 2D−A spin arrangement of Figure 3b in which the AFM alternating

(32) Lake, B.; Tennant, D. A. *Physica B* **1997**, 234−236, 557.
(33) Lake, B.; Cowley, R. A.; Tennant, D. A. *J. Phys.: Condens. Matter* **1997**, *9*, 10951.

chains made up of J_9(A) and J_1(A) run along [1 −1 −1]. (The 2D magnetic sheet of $Cu(Mo_{0.25}W_{0.75})O_4$ is also predicted to have the 2D−A spin arrangement, even if the path J_1(A) has a stronger tendency for AFM ordering than does the path J_8. In this case, the SISU's become the AFM alternating chains made up of J_9(A) and J_1(A) run along [1 −1 −1], and these chains will be coupled antiferromagnetically via the paths J_8 thereby leading to the 2D−A spin arrangement.)

The Δe value for the superexchange path J_1(B) of $Cu(Mo_{0.25}W_{0.75})O_4$ is similar in magnitude to that of $CuMoO_4$-III. Consequently, adjacent 2D magnetic sheets of $Cu(Mo_{0.25}W_{0.75})O_4$ are expected to be antiferromagnetically coupled via the superexchange paths J_1(B), as in $CuMoO_4$-III. Therefore, as shown in Figure 2d, the magnetic unit cell of $Cu(Mo_{0.25}W_{0.75})O_4$ should be doubled along the *a*-axis as well as along the *b*-axis.

Spin−Orbital Interaction Energy and Geometrical Parameters

In this section we examine how the trends in the Δe values of the exchange paths are related to their geometrical parameters. For the superexchange paths J_1(A) and J_1(B), important geometrical parameters are the Cu···Cu distance and the ∠Cu−O−Cu bond angle of their Cu−O−Cu bridges.[13,25] For the super-superexchange paths J_6(B), J_8, and J_9(A), important geometrical parameters are the O···O distance and the two ∠Cu−O···O bond angles of their Cu−O···O−Cu linkages. These geometrical parameters are summarized in Tables 2−4.

Let us first consider interchain spin dimers, in which two spin sites are connected by the super-superexchange paths Cu−O···O−Cu. For such a spin dimer the overlap between the magnetic orbitals occurs primarily through the overlap between their oxygen tails. As depicted in Figure 4a, the magnetic orbital is highly anisotropic in that the atomic orbital components are contained in the equatorial plane of the spin monomer and the oxygen p-orbital tails are pointed along the equatorial Cu−O bonds. Consequently, the overlap integral between the two magnetic orbitals depends on the two ∠Cu−O···O angles and the O···O contact distance. The consideration of the oxygen tails of the magnetic orbitals shows that the overlap integral at a given O···O distance would increase as the Cu−O···O linkage becomes more linear. The relative orientations of the two equatorial planes of the spin dimers associated with the exchange paths J_9(A), J_8, and J_6(B) are presented as stereoviews in Figure 5a−c, respectively. These reveal that the J_9(A) and J_8 paths each have one short O···O contact, while the J_6(B) path has three short O···O contacts. Tables 2−4 show that both ∠Cu−O···O angles are larger for the J_9(A) path than for the J_8 path (i.e., 166−168° versus 154−160°). In addition, the O···O contact distance considerably shorter for the J_9(A) path than for the J_8 path (by about 0.4 Å). Thus, the J_9(A) path has a much larger Δe value than does the J_8 path. The J_6(B) path has three short O···O contacts, but the associated ∠Cu−O···O angles are not favorable for good overlap between the oxygen tails of the two magnetic orbitals: in one O···O contact both ∠Cu−O···O angles are smaller than 110°, while in the remaining two O···O contacts one ∠Cu−O···O angle is smaller than 110°. As a result, the Δe value is smaller for the J_6(B) path than for the J_8 path despite the fact that the former has three short O···O contacts.

We now consider the intrachain spin dimers, in which spin sites are connected by the superexchange paths Cu−O−Cu. For each of $CuWO_4$, $CuMoO_4$-III and $Cu(Mo_{0.25}W_{0.75})O_4$, the ∠Cu−O−Cu angles deviate considerably from 90° (i.e., 97−99°) for the J_1(A) path but are close to 90° (i.e., 88−90°) for the J_1(B) path. Thus, the J_1(A) path has a larger Δe value than does the J_1(B) path in each compound and, hence, should have a tendency for AFM coupling. The ∠Cu−O−Cu bond angle of the J_1(B) path is practically 90° in $CuWO_4$ but slightly smaller than 90° in $CuMoO_4$-III and $Cu(Mo_{0.25}W_{0.75})O_4$. In addition, the Cu···Cu distance of the J_1(B) path is slightly longer in $CuWO_4$ than in $CuMoO_4$-III and $Cu(Mo_{0.25}W_{0.75})O_4$. These geometrical factors are consistent with the finding that the Δe value of the J_1(B) path is smaller for $CuWO_4$ than for $CuMoO_4$-III and $Cu(Mo_{0.25}W_{0.75})O_4$. However, on the basis of the geometrical parameters alone, it is not obvious why the Δe value of the J_1(A) path is much larger for $Cu(Mo_{0.25}W_{0.75})O_4$ than for $CuWO_4$ and $CuMoO_4$-III.

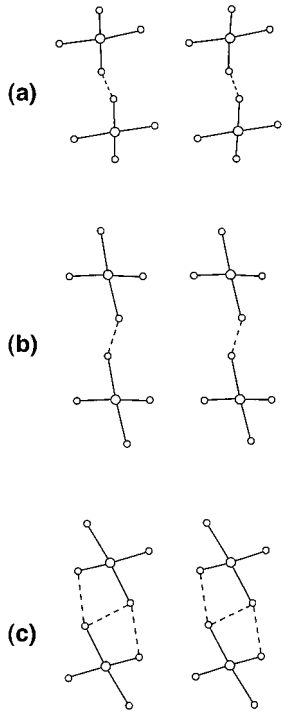

Figure 5. Stereoviews of how the two spin monomers of the interchain spin dimer are arranged in the exchange paths (a) J_9(A), (b) J_8, and (c) J_6(B). Here the large and small circles represent the Cu and O atoms, respectively. For each spin monomer, the two long axial Cu−O bonds are not shown, because the magnetic orbital does not have orbital contributions from the axial oxygen atoms. The short O···O contacts between the spin monomers are indicated by dashed lines.

Concluding Remarks

The magnetic structures of the distorted wolframite-type oxides $CuWO_4$, $CuMoO_4$-III, and $Cu(Mo_{0.25}W_{0.75})O_4$ are described in terms of the 2D magnetic sheets defined by one superexchange path, J_1(A), and three super-superexchange paths, J_6(B), J_8, and J_9(A). The SISU's of the 2D magnetic sheets are the AFM ladder chains defined by J_8 and J_9(A) running along [1 0 1], and short-range magnetic order in these ladder chains should be responsible for the broad maximum in the magnetic susceptibility of $CuWO_4$ at $T_{max} \approx 90$ K. The coupling between adjacent AFM ladder chains in a 2D magnetic sheet leads to spin frustration, so that adjacent AFM ladder chains can be coupled via the J_1(A) paths ferromagnetically to form the 2D−F spin arrangement (Figure 3a) or antiferromagnetically to form the 2D−A spin arrangement (Figure 3b). The 2D magnetic sheets of $CuWO_4$ and $CuMoO_4$-III have the 2D−F spin arrangement in which AFM alternating chains run along [2 −1 0], while those of $Cu(Mo_{0.25}W_{0.75})O_4$ are predicted to

adopt the 2D−A spin arrangement so that AFM alternating chains run along [1 −1 −1].

In $CuWO_4$, $CuMoO_4$-III, and $Cu(Mo_{0.25}W_{0.75})O_4$, adjacent 2D magnetic sheets interact via the superexchange paths J_1(B). The spin−orbital interaction energies calculated for J_1(B) support Ehrenberg et al.'s conclusion[7] that adjacent 2D magnetic sheets couple via J_1(B) ferromagnetically in $CuWO_4$ but antiferromagnetically in $CuMoO_4$-III and, hence, that the magnetic unit cell is doubled along the *a*-axis in $CuWO_4$ and along the *c*-axis in $CuMoO_4$-III. It is predicted that adjacent 2D magnetic sheets of $Cu(Mo_{0.25}W_{0.75})O_4$ couple via J_1(B) antiferromagnetically, and so its magnetic unit cell doubles along the *a*-axis as well as along the *b*-axis.

In understanding the magnitude of a super-superexchange interaction, it is essential to consider the geometrical parameters that control the overlap between the tails of the two magnetic orbitals, namely, the O···O distance and the two ∠Cu−O···O angles of the Cu−O···O−Cu bridge.

Acknowledgment. Work at North Carolina State University was supported by the Office of Basic Energy Sciences, Division of Materials Sciences, U.S. Department of Energy, under Grant DE-FG05-86ER45259. The authors thank Dr. H. Ehrenberg for references and information about the crystal structures of $CuMoO_4$-III and $Cu(Mo,W)O_4$.

IC001445R